Systematic Uncertainties in E89-003

A Report to the Hall A Collaboration

Kevin Fissum
Lund University
SE-221 00 Lund
Sweden
kevin.fissum@nuclear.lu.se

Paul Ulmer
Old Dominion University
Norfolk, VA, 23529
USA
ulmer@jlab.org

Abstract

The systematic uncertainties for the cross section measurements performed during Hall A experiment E89-003 were investigated. These uncertainties were classified into two catergories: scale and kinematic-dependent. Scale systematic uncertainties were extracted from the archives. They were determined to dominate. An exhaustive series of simulations was performed to quantify the kinematic-dependent effects. They were determined to be small. The average systematic uncertainty associated with a $1p$-shell cross section is estimated to be 5.6%, while that associated with a continuum cross section is estimated to be 5.9%. These results are comparable with those obtained in similar analyses. A complete overview of the investigation is presented.

JLAB-TN-02-015 *24 April 2002*

Contents

1 Overview

The oxygen cross sections we reported for E89-003, whether they were bound-state (5-fold differential) or continuum (6-fold differential), were extracted using

$$\sigma = \left(\frac{\sigma_{Mainz}}{\sigma_H}\right) \cdot \sigma_O, \tag{1}$$

where σ_{Mainz} is the Mainz form-factor parametrization of the $^1\mathrm{H}(e,e)$ cross section [1], and σ_H and σ_O were the measured $^1\mathrm{H}(e,e)$ and $^{16}\mathrm{O}(e,e'p)$ cross sections. Some of the variables which appear in our measured cross sections contribute kinematic-independent (that is, overall scale) systematic uncertainties to our results, while others contribute systematic uncertainties which are a function of the particular setup in question.

This document presents our estimation of the systematic uncertainties of the E89-003 cross section data points for the upcoming PRC article. Our approach to evaluating these uncertainties has been to thoroughly review the experimental uncertainties identified in all the previous writeups (such as the technotes, the theses, and the PRL-style articles [2–10]), and then to investigate the intrinsic behavior of the cross sections when constituent parameters are varied over the appropriate experimentally determined ranges using the de facto Hall A simulation package `MCEEP` [11]. These `MCEEP` simulations incorporate the latest calculations of J. M. Udías [12] *et al.* (see Appendix A), and are based on the data of E89-003 [13]. In evaluating the simulation results, the cuts applied in the data analyses were also applied to the pseudo-data, and the cross sections were evaluated for the identical P_{miss} bins used to present the results (see Appendix B). The uncertainties so-determined were also examined for convergence.

The interested reader is directed to the detailed discussion of the error analysis and propagation techniques employed in this document that is presented in [14].

2 Cross section uncertainties

2.1 Motivation

In order to estimate the systematic uncertainty in the reported cross sections, we rewrite (1) as

$$\sigma = \sigma_{Mainz} \cdot \left(\frac{\sigma_O}{\sigma_H}\right); \tag{2}$$

that is,

$$\sigma = \sigma(\sigma_{Mainz}, \frac{\sigma_O}{\sigma_H}). \tag{3}$$

Here, σ_O is given by

$$\sigma_O = \sigma_O(\eta_{DAQ}, \eta_{elec}, \rho t', N_e, \epsilon_e\epsilon_p\epsilon_{coin}, \Delta\Omega_e, \Delta\Omega_p, R_O, \Delta V_O), \tag{4}$$

where η_{DAQ} is the data acquisition deadtime, η_{elec} is the electronics deadtime, R_O is the radiative correction applied to the data, $\rho t'$ is the effective target thickness, N_e is the number of incident electrons, $\epsilon_e\epsilon_p\epsilon_{coin}$ is the overall trigger efficiency, $\Delta\Omega_e$ is the solid angle subtended by the HRS$_e$, $\Delta\Omega_p$ is the solid angle subtended by the HRS$_h$, and ΔV_O is the phase space volume subtended by the bin for which σ_O was evaluated. Similarly, σ_H is given by

$$\sigma_H = \sigma_H(\eta_{DAQ}, \eta_{elec}, \rho t', N_e, \epsilon_e, \Delta\Omega_e, R_H, \Delta V_H), \tag{5}$$

where all of the variables have already been defined in the vicinity of (4) save R_H (the radiative correction applied to the data) and ΔV_H, which is the phase space volume element for which σ_H was evaluated. Note that ΔV_O and ΔV_H were *never* identical.

Since σ_O and σ_H were measured simultaneously, certain identical quantities appear in both the numerator and the denominator of the bracketed term of (2). These terms (namely η_{DAQ}, η_{elec}, $\rho t'$, N_e, ϵ_e, and $\Delta\Omega_e$) individually set the absolute normalizations of the σ_O and σ_H cross sections. Because we normalized our results to σ_{Mainz}, these terms simply drop out of the calculation of σ, such that

$$\frac{\sigma_O}{\sigma_H} = \frac{\sigma_O}{\sigma_H}(R_O, R_H, \epsilon_p\epsilon_{coin}, \Delta\Omega_p; \Delta V_O, \Delta V_H). \tag{6}$$

Thus, the functional dependency of our quoted cross sections is given by

$$\sigma = \sigma(\sigma_{Mainz}, R_O, R_H, \epsilon_p\epsilon_{coin}, \Delta\Omega_p; \Delta V_O, \Delta V_H). \tag{7}$$

We expand (7) as:

$$\left(\frac{\delta\sigma}{\sigma}\right)^2 = \overbrace{\left(\frac{\delta\sigma_{Mainz}}{\sigma_{Mainz}}\right)^2 + \left(\frac{\delta R_O}{R_O}\right)^2 + \left(\frac{\delta R_H}{R_H}\right)^2 + \left(\frac{\delta\epsilon_p\epsilon_{coin}}{\epsilon_p\epsilon_{coin}}\right)^2 + \left(\frac{\delta\Delta\Omega_p}{\Delta\Omega_p}\right)^2}^{\text{scale uncertainties}} + \underbrace{\left(\frac{\delta V(\Delta V_O, \Delta V_H)}{V(\Delta V_O, \Delta V_H)}\right)^2}_{\text{kinematic-dependent uncertainties}}. \tag{8}$$

The first five terms in (8) are orthogonal scale systematic uncertainties.[1] The dependences of the cross section on beam energy and direction, electron and proton angle, and electron and proton momentum all appear within the phase space volume elements

$$\Delta V_O = \Delta V_O(E_{\text{beam}}, \phi_{\text{beam}}, \theta_{\text{beam}}, p_e, \phi_e, \theta_e, p_p, \phi_p, \theta_p) \tag{9}$$

$$\Delta V_H = \Delta V_H(E_{\text{beam}}, \phi_{\text{beam}}, \theta_{\text{beam}}, p_e, \phi_e, \theta_e), \tag{10}$$

where E_{beam} is the energy of the beam, ϕ_{beam} is the beam in-plane angle, θ_{beam} is the beam out-of-plane angle, p_e (p_p) is the electron (proton) momentum, ϕ_e (ϕ_p) is the in-plane angle of the scattered electron (proton), and θ_e (θ_p) is the out-of-plane angle of the scattered electron (proton).

The kinematic-dependent systematic uncertainties for the phase-space volume elements ΔV_O and ΔV_H are difficult to assess directly. We thus relied upon simulation (see 2.2.2).

[1] At first glance, it may be surprising to note that the uncertainty due to the radiative correction to the data is included as a scale uncertainty. In general, the radiative correction is strongly dependent on kinematics. However, the E89-003 $1p$-shell data analysis, and for that matter any bound-state data analysis, involves missing mass cuts. These cuts to a large extent remove the strong kinematic dependence of the radiative correction, since only relatively small photon energies are involved. This behavior has been observed in independent analyses of other experiments. In order to compensate for any remaining weak kinematic dependence, the uncertainty due to the radiative correction was slightly overestimated.

2.2 Uncertainties

Information on the experimental uncertainties has been extracted from the various writeups associated with E89-003. Some of these values are quoted directly in the following section as scale uncertainties, while the remainder served as input to the `MCEEP` simulation suite.

2.2.1 Scale uncertainties

In Table 1, we summarize the values extracted from the references for the scale systematic uncertainties which contribute to σ_O and σ_H. As previously discussed, the first seven entries do not contribute to the systematic uncertainties in the reported cross sections - they have been included for completeness.

Quantity	δ (%)
η_{DAQ}	2.0
η_{elec}	<1.0
$\rho t'$	2.5
N_e	2.0
ϵ_e	1.0
$\Delta\Omega_e$	2.0
$\epsilon_e\epsilon_p\epsilon_{coin}$	1.5
σ_{Mainz}	4.0
R_O	2.0
R_H	2.0
$\epsilon_p\epsilon_{coin}$	<1.0
$\Delta\Omega_p$	2.0

Table 1
Summary of the scale systematic uncertainties contributing to σ_O and σ_H. The first seven entries do not contribute to the systematic uncertainties in the reported cross sections.

The quadratic sum of the last five entries is 5.4%, clearly dominated by the 4.0% systematic uncertainty in the σ_{Mainz} normalization procedure. For details regarding the evaluation of the uncertainty in this procedure, the interested reader is directed to Appendix C.

2.2.2 Kinematic-dependent uncertainties

New utilities were written for and incorporated into `MCEEP`, which was then used to investigate the intrinsic behavior of σ_O and σ_H when constituent kinematic parameters were varied over the appropriate experimentally determined ranges.

A new auxiliary program `systerr`[2] uses a `MCEEP`-generated `Ntuple` of target `Transport` coordinates (ϕ, θ, and δ for each spectrometer arm) as input. For each `Ntuple` event, it calculates the nominal $(e, e'p)$ cross section. Nine additional cross sections are also calculated, each corresponding to a standard (1 mr or 10^{-3}) shift of one of nine kinematic quantities (the horizontal and vertical angles and the magnitude of the momentum for the beam, scattered electron, and ejectile). These ten newly calculated cross sections are then attached to the original `Ntuple` event, so that the output `Ntuple` contains these *in addition to* all the variables in the original input `Ntuple`. This method has the advantage that the same statistical sample is used for all ten cross sections, as might not be the case when the cross sections are obtained from subsequent runs of `MCEEP`. In this manner, reasonably precise kinematic derivatives are obtained with a relatively small statistical sample.

Another new auxiliary program `toterr` was then used to calculate the total systematic uncertainty from all kinematic sources based on the actual kinematic uncertainties (see Table 2) and including any appropriate correlations between variables as specified by the user. We exploited the experimental constraints to the kinematic-dependent observables afforded us by the overdetermined ^{1}H(e, ep) reaction to "calibrate" or "constrain" the experimental setup. We chose as our independent parameters the in-plane electron and proton angles ϕ_e and ϕ_p. When a known shift in ϕ_e was made, ϕ_p was held constant and the complementary variables $E_{\rm beam}$, p_e, and p_p were varied as required by the constraints enforced by the ^{1}H(e, ep) reaction. Similarly, when a known shift in ϕ_p was made, ϕ_e was held constant and the complementary variables $E_{\rm beam}$, p_e, and p_p were varied as appropriate. The overall constrained uncertainty is taken to be the quadratic sum of the two contributions.

Table 2 presents a summary of the systematic uncertainties used as input to the `MCEEP` simulation suite. Uncertainty due to the variations in the in-plane incident beam angle was ignored.[3]

---

[2] This program is linked to the `MCEEP` subroutines so that any improvements in or additions to the physics model libraries within `MCEEP` will also be available to `systerr`.

[3] The angle of incidence of the electron beam was determined using a pair of beam position monitors (BPMs) located upstream of the target. The BPM readback was calibrated by comparing the location of survey fiducials along the beamline to the Hall A survey fiducials. Thus, in principle, uncertainty in the knowledge of the

Quantity	δ
$E_{\rm beam}$	1.6×10^{-3}
$\phi_{\rm beam}$	ignored
$\theta_{\rm beam}$	2.0 mr
p_e	1.5×10^{-3}
ϕ_e	0.3 mr
θ_e	2.0 mr
p_p	1.5×10^{-3}
ϕ_p	0.3 mr
θ_p	2.0 mr

Table 2
Systematic uncertainties folded into the `MCEEP` simulation suite.

The ^{16}O$(e,e'p)$ simulations incorporated the latest calculations of J. M. Udías *et al.* as physics input (see Appendix A), which are based on the actual data taken during E89-003. For each kinematics, the central water foil was considered, and 1M events were generated. The global convergence of the uncertainty estimate was examined for certain extreme kinematics, where 10M-event simulations (which demonstrated the same behavior) were performed. In evaluating the simulation results, the exact cuts applied in the actual data analyses were also applied to the pseudo-data, and the cross sections were evaluated for the identical $P_{\rm miss}$ bins used to present the results (see Appendix B). The behavior of the uncertainty as a function of $P_{\rm miss}$ was also investigated by examining the uncertainty in the momentum bins adjacent to the reported momentum bin in exactly the same fashion. Interested parties may obtain the results of the simulations (roughly 45 Gb of `.hbook` files) from the authors.

The kinematically induced systematic uncertainty in σ_O is presented in Table 3. This uncertainty was calculated as a quadratic sum of the values presented in Tables D.1, D.2, and D.3 from Appendix D.1.1. While the magnitude of these uncertainties is small, they do depend upon $P_{\rm miss}$. Based on the data, we modelled the high-E$_{\rm miss}$ region as the superposition of a peak-like $1s_{1/2}$-state on a flat continuum. Contributions to the systematic uncertainty from the flat continuum were taken to be small, leaving only those from the $1s_{1/2}$-state. Values labelled with a '†' should not be taken too seriously due to the

incident electron beam angle should be included in this analysis. However, our simultaneous measurement of the overdetermined ^{1}H(e,ep) reaction allowed us to "calibrate" our kinematics absolutely, and thus eliminate this uncertainty. That is, the direction of the beam defined the axis relative to which all angles are measured via ^{1}H(e,ep).

lack of knowledge of the $1s_{1/2}$-state spectral function for $|\theta_{pq}| > 8°$.

		$\delta(d^5\sigma/d\omega d\Omega_e d\Omega_p)$		$\delta(d^6\sigma/d\omega dE_p d\Omega_e d\Omega_p)$
$E_{\rm beam}$	θ_{pq}	$1p_{1/2}$-state	$1p_{3/2}$-state	continuum
(GeV)	(°)	(%)	(%)	(%)
0.843	0	0.4	0.3	0.4
	8	1.4	1.2	1.7
	16	2.8	4.7	1.2†
	-8	0.9	0.8	1.2
1.642	0	0.8	0.7	0.2
	8	1.2	0.5	1.5
	-20	1.3	0.5	1.2†
	-16	1.7	2.9	1.0†
	-8	1.1	0.9	1.5
2.442	0	1.2	1.2	0.3
	2.5	0.7	0.9	0.8
	8	1.2	1.0	1.4
	16	1.8	3.0	0.7†
	20	1.5	0.8	1.4†

Table 3
Quadratic sum of the kinematic-dependent systematic uncertainties for σ_O which contribute to σ. The constraints provided by ^{1}H(e,ep) have been considered in the above. The $P_{\rm miss}$ bins for which cross sections are reported are presented in Appendix B. While the magnitude of these uncertainties is small, they exhibit clear dependence on $P_{\rm miss}$. Values labelled with a '†' should not be taken too seriously due to the lack of knowledge of the $1s_{1/2}$-state spectral function for $|\theta_{pq}| > 8°$. An archive of the terms contributing to these results is presented in Appendix D.1.1.

The kinematically induced systematic uncertainty in σ_H is presented in Appendix D.2 in Table D.10. It is negligible.

2.3 Summary of results

Table 4 presents our best estimate of the overall systematic uncertainties associated with our various cross section measurements for E89-003. Uncertainties presented in Tables 1 and 3 have been combined in quadrature to obtain these

results. An additional 2% uncertainty has been attributed to the continuum results due to the collimator punch-through correction.

		$\delta(d^5\sigma/d\omega d\Omega_e d\Omega_p)$		$\delta(d^6\sigma/d\omega dE_p d\Omega_e d\Omega_p)$
$E_{\rm beam}$	θ_{pq}	$1p_{1/2}$-state	$1p_{3/2}$-state	continuum
(GeV)	(°)	(%)	(%)	(%)
0.843	0	5.4	5.4	5.8
	8	5.6	5.5	6.0
	16	6.1	7.2	5.9†
	-8	5.5	5.5	5.9
1.642	0	5.5	5.4	5.8
	8	5.5	5.4	6.0
	-20	5.5	5.4	5.9†
	-16	5.7	6.1	5.8†
	-8	5.5	5.5	6.0
2.442	0	5.5	5.5	5.8
	2.5	5.4	5.5	5.8
	8	5.5	5.5	5.9
	16	5.7	6.2	5.8†
	20	5.6	5.5	5.9†

Table 4
Estimated systematic uncertainties for the reported cross sections. The $P_{\rm miss}$ bins for which cross sections are reported are presented in Appendix B. Values labelled with a '†' should not be taken too seriously due to the lack of knowledge of the $1s_{1/2}$-state spectral function for $|\theta_{pq}| > 8°$.

The average systematic uncertainty for the $1p$-shell results is 5.6%. The average systematic uncertainty for the continuum results is 5.9%. In both cases, the variation of the kinematic-dependent systematic uncertainty with $P_{\rm miss}$ is washed out by the much larger contribution of the scale systematic uncertainties. All uncertainties are dominated by the 4% uncertainty attributed to the σ_{Mainz} normalization procedure.

Ultimately, we verified that enforcing the ^{1}H(e,ep) "constraints" upon the data in the analysis strongly dampened the kinematic-dependent systematic uncertainties for the E89-003 results. Neither the restrictive acceptance cuts, the small $P_{\rm miss}$ bins, nor the point-source target had much effect upon the kinematic-dependent uncertainties. [4]

ACKNOWLEDGEMENTS

We acknowledge the valuable contributions to this work made by J. W. Van Orden (who provided the first-generation RPWIA calculations incorporated into `MCEEP`), J. M. Udías (who provided the latest RDWIA calculations used for the simulation suite), and L. B. Weinstein (who participated in many helpful discussions).

[4] While not directly mentioned in the main text, certain of the "unconstrained" systematic uncertainties are presented in Appendix D.1.2. They are large.

References

[1] G. Simon *et al.*, Absolute Electron-Proton Cross Sections at Low Momentum Transfer Measured With a High Pressure Gas Target System, Nucl. Phys. **A333**, 381 (1980).

[2] K. Fissum *et al.*, Study of the Quasielastic $(e, e'p)$ Reaction in ^{16}O at High Recoil Momentum, MIT-LNS Internal Report #02, 1997.

[3] P. Ulmer, Requirements on the Determination of the Beam Energy for E89-003, Old Dominion University Internal Report, 1997.

[4] J. Gao *et al.*, Beam Energy Measurement at JLab Using the Hall A Spectrometers, MIT-LNS Internal Report #04, 1998.

[5] N. Liyanage *et al.*, Optics Commissioning of the Hall A High Resolution Spectrometers, MIT-LNS Internal Report #05, 1998.

[6] P. Ulmer, Beam Charge Measurements for Hall A Experiment E89-003 at JLab, Old Dominion University Internal Report, 1998.

[7] J. Gao, Study of Quasielastic $1p$-shell Proton Knockout in the ^{16}O$(e, e'p)$ Reaction at $Q^2 = 0.8$ (GeV/c)^2, MIT Ph.D. thesis, 1999.

[8] N. Liyanage, A Study of the ^{16}O$(e, e'p)$ Reaction at Deep Missing Energies, MIT Ph.D. thesis, 1999.

[9] J. Gao *et al.*, Dynamical Relativistic Effects in Quasielastic $1p$-Shell Proton Knockout from ^{16}O, Phys. Rev. Lett. **84**, 3265 (2000).

[10] N. Liyanage *et al.*, Dynamics of the ^{16}O$(e, e'p)$ Reaction at High Missing Energies, Phys. Rev. Lett. **86**, 5670 (2001).

[11] P. Ulmer, Monte Carlo for $(e, e'p)$, `http://www.physics.odu.edu/~ulmer/mceep/mceep.html`.

[12] J. M. Udías, private communication.

[13] `http://www.jlab.org/~fissum/e89003.html`

[14] L. Lyons, *A Practical Guide to Data Analysis for Physical Science Students*, Cambridge University Press, 1991.

[15] P. E. Ulmer *et al.*, The quasielastic ^{2}H$(e, e'p)$n reaction at high recoil momenta, submitted to *Physical Review Letters* in 2001.

[16] *Conceptual Design Report, Basic Experimental Equipment*, Internal Report, CEBAF, 1990 (unpublished).

[17] J. W. Van Orden, private communication to Paul Ulmer.

[18] N. Liyanage, private communication.

Appendices

A The latest Udías *et al.* calculations

Figs. A.1, A.2, and A.3 show the latest Udías *et al.* RDWIA calculations for the $1p_{1/2}$-, $1p_{3/2}$-, and $1s_{1/2}$-states of ^{16}O compared to the older Van Orden *et al.* [17] RPWIA calculations we used for the rate estimates for E89-003. These latest calculations are based on the $1p$-shell data from E89-003. They were recently incorporated into `MCEEP`. As can be seen, the RPWIA calculations from the two authors are quite similar. Note that while the RPWIA curves require an external spectroscopic factor to obtain agreement with experimental data, the RDWIA calculations already contain this normalization.

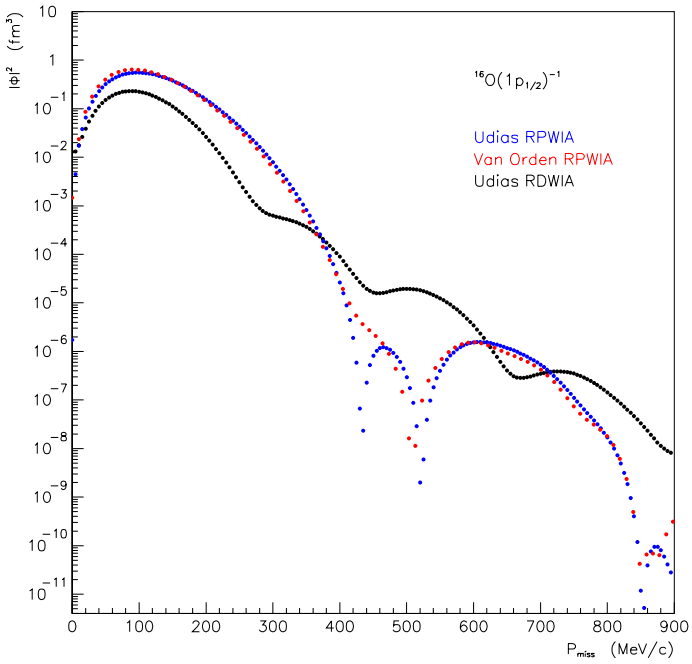

Fig. A.1. Udías *et al.* RDWIA calculation for the $1p_{1/2}$-state of ^{16}O based on $1p$-shell data from E89-003. Also shown are the older Van Orden *et al.* calculations we used for the rate estimates for E89-003.

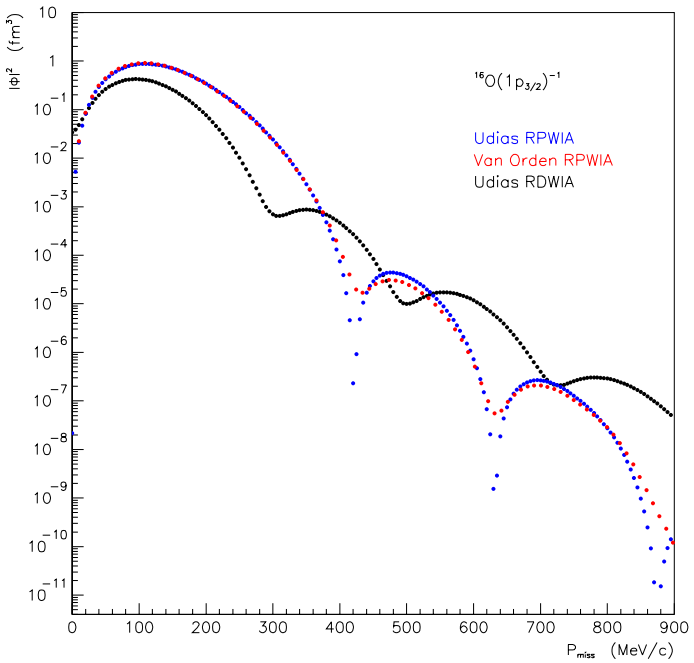

Fig. A.2. Udías *et al.* RDWIA calculation for the $1p_{3/2}$-state of ^{16}O based on $1p$-shell data from E89-003. Also shown are the older Van Orden *et al.* calculations we used for the rate estimates for E89-003.

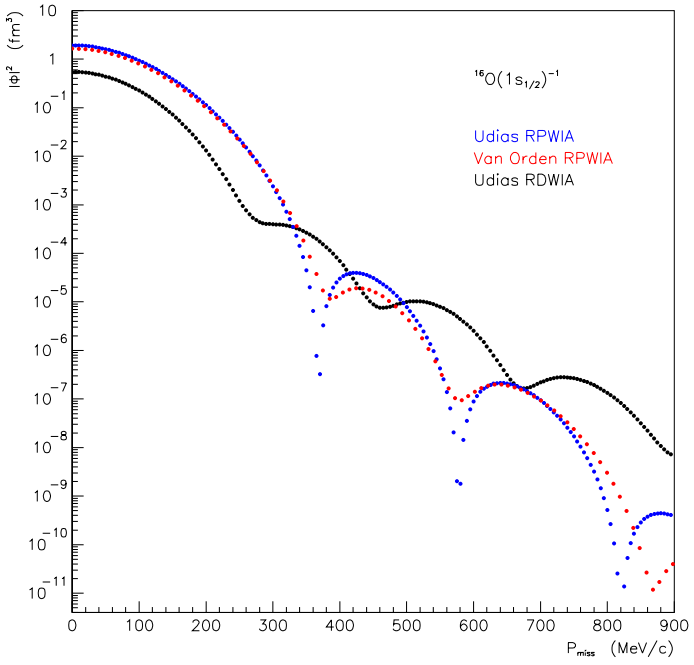

Fig. A.3. Udías *et al.* RDWIA calculation for the $1s_{1/2}$-state of ^{16}O based on $1p$-shell data from E89-003. Also shown are the older Van Orden *et al.* calculations we used for the rate estimates for E89-003.

B Pseudo-data cuts and bins

Table B.1 summarizes the center waterfilm central acceptance cuts determined during the data analysis and used in the simulation suite.

HRS	θ (mr)	ϕ (mr)	δ (%)
e	$[-50, +45]$	$[-26, +24]$	$[-3.7, +3.3]$
h	$[-50, +50]$	$[-22, +22]$	$[-3.7, +3.3]$

Table B.1
A summary of the central acceptance cuts.

For the analysis and simulation of the $^{1}\mathrm{H}(e,e)$ data, yields were integrated over all events surviving the cuts presented in Table B.1. For the analysis and simulation of the $^{16}\mathrm{O}(e,e'p)$ data, yields which survived the cuts presented in Table B.1 were integrated for the P_{miss} bins presented in Table B.2.

E_{beam}	θ_{pq}	$< P_{\mathrm{miss}} >$ (MeV/c)	
(GeV)	(°)	$1p$-shell	continuum
0.843	0	52.5	42.5
	8	149.0	145.0
	16	275.0	280.0
1.642	-8	149.0	145.0
	0	52.5	42.5
	8	149.0	145.0
2.442	-20	342.5	340.0
	-16	275.0	280.0
	-8	149.0	145.0
	0	52.5	42.5
	2.5	60.0	50.0
	8	149.0	145.0
	16	275.0	280.0
	20	342.5	340.0

Table B.2
A summary of the $^{16}\mathrm{O}(e,e'p)$ central P_{miss} values in MeV/c. The $1p$-shell bins were 20 MeV/c wide, while the continuum bins were 5 MeV/c wide.

C σ_{Mainz}

Fig. C.1 shows the agreement between the ^{1}H(e,e) cross sections measured during E89-003 and the predictions of the Mainz parameterization. Based on these results, a systematic uncertainty of 4% was assigned to the overall σ_{Mainz} normalization procedure [18].

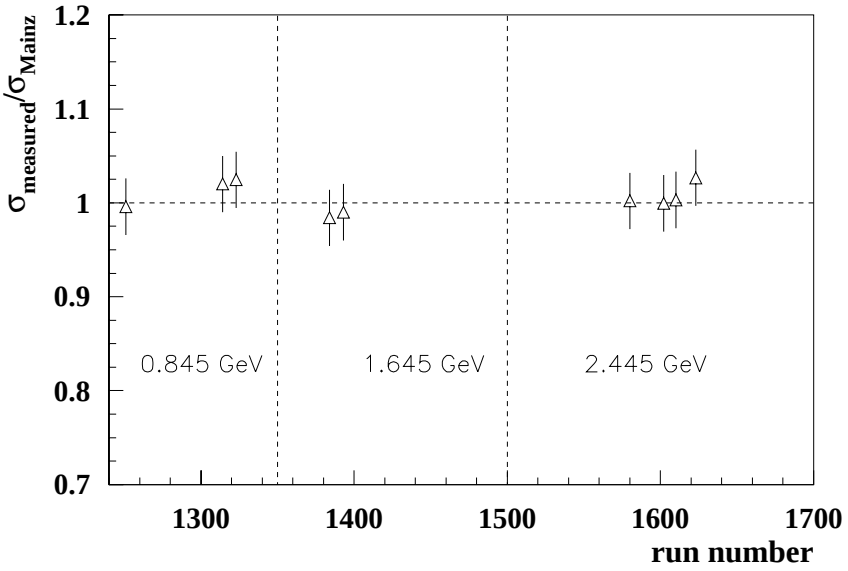

Fig. C.1. The measured ^{1}H(e,e) cross sections for E89-003 [13] normalized to the absolute value predicted by the Mainz parameterization [1]. The vertical bars delineate regions labelled by the nominal beam energies. Figure courtesy N. Liyanage.

D `MCEEP` simulation results

The following tables present a comprehensive summary of the kinematic-dependent systematic uncertainties. In all cases, 1M events were modeled. The exact cuts applied to the experimental data in the data analyses were also applied to the pseudo-data, and the cross sections were then extracted for the same $P_{\rm miss}$ bins used for the publishing of the results. Results quoted for the continuum were extracted by running the simulations for the $1s_{1/2}$-state, and values labelled with a '†' should not be taken too seriously due to the lack of knowledge of the $1s_{1/2}$-state spectral function for $|\theta_{pq}| > 8°$.

D.1 $^{16}\mathrm{O}(e,e'p)$

D.1.1 Constrained results

In general, uncertainties in the cross sections due to uncertainty in the absolute in-plane electron angle were smaller than those due to uncertainty in the absolute in-plane proton angle. Cross-section uncertainties due to out-of-plane uncertainties were very small.

		$\delta(d^5\sigma/d\omega d\Omega_e d\Omega_p)$		$\delta(d^6\sigma/d\omega dE_p d\Omega_e d\Omega_p)$
E_{beam}	θ_{pq}	$1p_{1/2}$-state	$1p_{3/2}$-state	continuum
(GeV)	(°)	(%)	(%)	(%)
0.843	0	0.2	0.1	0.3
	8	0.5	0.4	0.6
	16	0.9	1.5	0.5†
	-8	0.5	0.5	0.7
1.642	0	0.7	0.7	0.1
	8	0.4	0.4	0.6
	-20	1.1	0.4	1.1†
	-16	1.2	1.9	0.8†
	-8	0.8	0.7	1.2
2.442	0	1.2	1.2	0.1
	2.5	0.6	0.5	0.7
	8	0.4	0.5	0.5
	16	0.3	0.5	0.4†
	20	0.8	0.7	0.8†

Table D.1
Uncertainties in the $^{16}\mathrm{O}(e,e'p)$ cross sections due to an uncertainty in the absolute in-plane electron angle of 0.3 mr. The constraints provided by $^{1}\mathrm{H}(e,ep)$ have been considered in the above. The P_{miss} bins for which cross sections are reported are presented in Appendix B. Values labelled with a '†' should not be taken too seriously due to the lack of knowledge of the $1s_{1/2}$-state spectral function for $|\theta_{pq}| > 8°$.

$E_{\rm beam}$ (GeV)	θ_{pq} (°)	$\delta(d^5\sigma/d\omega d\Omega_e d\Omega_p)$ $1p_{1/2}$-state (%)	$1p_{3/2}$-state (%)	$\delta(d^6\sigma/d\omega dE_p d\Omega_e d\Omega_p)$ continuum (%)
0.843	0	0.1	0.2	0.2
	8	1.3	1.1	1.6
	16	2.6	4.5	1.1†
	-8	0.8	0.6	0.9
1.642	0	0.1	0.1	0.2
	8	1.1	0.3	1.4
	-20	0.6	0.2	0.5†
	-16	1.2	2.1	0.5†
	-8	0.8	0.6	0.9
2.442	0	0.1	0.1	0.2
	2.5	0.4	0.5	0.4
	8	1.1	0.9	1.3
	16	1.7	2.9	0.5†
	20	1.2	0.2	1.1†

Table D.2
Uncertainties in the ^{16}O$(e,e'p)$ cross sections due to an uncertainty in the absolute in-plane proton angle of 0.3 mr. The constraints provided by ^{1}H(e,ep) have been considered in the above. The $P_{\rm miss}$ bins for which cross sections are reported are presented in Appendix B. Values labelled with a '†' should not be taken too seriously due to the lack of knowledge of the $1s_{1/2}$-state spectral function for $|\theta_{pq}| > 8°$.

$E_{\rm beam}$ (GeV)	θ_{pq} (°)	$\delta(d^5\sigma/d\omega d\Omega_e d\Omega_p)$ $1p_{1/2}$-state (%)	$1p_{3/2}$-state (%)	$\delta(d^6\sigma/d\omega dE_p d\Omega_e d\Omega_p)$ continuum (%)
0.843	0	0.3	0.2	0.2
	8	0.1	0.1	0.1
	16	0.1	0.1	0.1†
	-8	0.1	0.1	0.2
1.642	0	0.3	0.2	0.1
	8	0.2	0.2	0.1
	-20	0.1	0.1	0.1†
	-16	0.1	0.4	0.2†
	-8	0.1	0.1	0.3
2.442	0	0.2	0.1	0.2
	2.5	0.1	0.6	0.2
	8	0.4	0.2	0.1
	16	0.5	0.7	0.2†
	20	0.2	0.4	0.1†

Table D.3
Uncertainties in the ^{16}O$(e,e'p)$ cross sections due to an uncertainty in the out-of-plane beam, electron, and proton angles of 2.0 mr added in quadrature. The constraints provided by ^{1}H(e,ep) have been considered in the above. The $P_{\rm miss}$ bins for which cross sections are reported are presented in Appendix B. Values labelled with a '†' should not be taken too seriously due to the lack of knowledge of the $1s_{1/2}$-state spectral function for $|\theta_{pq}| > 8°$.

D.1.2 Unconstrained results

In general, uncertainties in the cross sections due to uncertainty in the beam energy dominated. Uncertainties in the cross sections due to uncertainty in the absolute in-plane electron angle were smaller than those due to uncertainty in the absolute in-plane proton angle. Uncertainties in the cross sections due to uncertainty in the absolute electron momentum were larger than those due to uncertainty in the absolute proton momentum.

$E_{\rm beam}$ (GeV)	θ_{pq} (°)	$\delta(d^5\sigma/d\omega d\Omega_e d\Omega_p)$ $1p_{1/2}$-state (%)	$1p_{3/2}$-state (%)	$\delta(d^6\sigma/d\omega dE_p d\Omega_e d\Omega_p)$ continuum (%)
0.843	0	2.2	2.3	3.0
	8	1.1	0.9	2.1
	16	2.6	4.6	1.2†
	-8	4.3	3.5	4.5
1.642	0	2.6	3.0	1.3
	8	3.4	2.7	5.3
	-20	4.6	0.3	4.0†
	-16	10.5	18.0	4.3†
	-8	7.4	5.9	7.8
2.442	0	3.5	4.7	2.8
	2.5	5.2	6.9	0.4
	8	5.0	4.0	7.9
	16	10.5	19.1	3.7†
	20	4.8	1.9	4.4†

Table D.4
Uncertainties in the ^{16}O$(e,e'p)$ cross sections due to an uncertainty in the absolute beam energy of 1.6×10^{-3}. The constraints provided by ^{1}H(e,ep) have not been considered in the above. The $P_{\rm miss}$ bins for which cross sections are reported are presented in Appendix B. Values labelled with a '†' should not be taken too seriously due to the lack of knowledge of the $1s_{1/2}$-state spectral function for $|\theta_{pq}| > 8°$.

$E_{\rm beam}$ (GeV)	θ_{pq} (°)	$\delta(d^5\sigma/d\omega d\Omega_e d\Omega_p)$ $1p_{1/2}$-state (%)	$1p_{3/2}$-state (%)	$\delta(d^6\sigma/d\omega dE_p d\Omega_e d\Omega_p)$ continuum (%)
0.843	0	0.2	0.1	0.2
	8	0.2	0.2	0.3
	16	0.3	0.6	0.2†
	-8	0.3	0.3	0.5
1.642	0	0.5	0.4	0.5
	8	0.2	0.2	0.3
	-20	0.7	0.3	0.7†
	-16	1.0	1.7	0.7†
	-8	0.6	0.5	0.9
2.442	0	0.7	0.6	0.3
	2.5	0.3	0.3	0.3
	8	0.2	0.2	0.3
	16	0.3	0.3	0.4†
	20	0.4	0.4	0.4†

Table D.5

Uncertainties in the ^{16}O$(e,e'p)$ cross sections due to an uncertainty in the absolute electron angle of 0.3 mr. The constraints provided by ^{1}H(e,ep) have not been considered in the above. The $P_{\rm miss}$ bins for which cross sections are reported are presented in Appendix B. Values labelled with a '†' should not be taken too seriously due to the lack of knowledge of the $1s_{1/2}$-state spectral function for $|\theta_{pq}| > 8°$.

$E_{\rm beam}$ (GeV)	θ_{pq} (°)	$\delta(d^5\sigma/d\omega d\Omega_e d\Omega_p)$ $1p_{1/2}$-state (%)	$1p_{3/2}$-state (%)	$\delta(d^6\sigma/d\omega dE_p d\Omega_e d\Omega_p)$ continuum (%)
0.843	0	0.1	0.2	0.2
	8	0.4	0.3	0.6
	16	0.9	1.7	0.3†
	-8	0.7	0.6	0.9
1.642	0	0.5	0.1	0.1
	8	0.5	0.3	0.6
	-20	0.6	0.5	0.5†
	-16	1.0	1.8	0.5†
	-8	0.7	0.6	0.8
2.442	0	0.1	0.5	0.1
	2.5	0.3	0.4	0.6
	8	0.4	0.3	0.6
	16	0.9	1.8	0.3†
	20	0.3	0.2	0.3†

Table D.6
Uncertainties in the ^{16}O$(e,e'p)$ cross sections due to an uncertainty in the absolute proton angle of 0.3 mr. The constraints provided by ^{1}H(e,ep) have not been considered in the above. The $P_{\rm miss}$ bins for which cross sections are reported are presented in Appendix B. Values labelled with a '†' should not be taken too seriously due to the lack of knowledge of the $1s_{1/2}$-state spectral function for $|\theta_{pq}| > 8°$.

$E_{\rm beam}$ (GeV)	θ_{pq} (°)	$\delta(d^5\sigma/d\omega d\Omega_e d\Omega_p)$ $1p_{1/2}$-state (%)	$1p_{3/2}$-state (%)	$\delta(d^6\sigma/d\omega dE_p d\Omega_e d\Omega_p)$ continuum (%)
0.843	0	0.4	0.3	0.5
	8	0.7	0.5	0.8
	16	1.2	2.3	0.3†
	-8	4.3	3.6	5.1
1.642	0	1.0	0.9	1.0
	8	2.6	2.0	3.8
	-20	5.1	0.2	4.4†
	-16	9.6	16.6	4.2†
	-8	6.9	5.7	7.8
2.442	0	0.8	1.6	2.0
	2.5	4.3	4.7	0.1
	8	4.0	3.1	6.3
	16	9.6	17.5	3.4†
	20	3.4	2.4	3.0†

Table D.7
Uncertainties in the ^{16}O$(e,e'p)$ cross sections due to an uncertainty in the absolute electron momentum of 1.5×10^{-3}. The constraints provided by ^{1}H(e,ep) have not been considered in the above. The $P_{\rm miss}$ bins for which cross sections are reported are presented in Appendix B. Values labelled with a '†' should not be taken too seriously due to the lack of knowledge of the $1s_{1/2}$-state spectral function for $|\theta_{pq}| > 8°$.

$E_{\rm beam}$ (GeV)	θ_{pq} (°)	$\delta(d^5\sigma/d\omega d\Omega_e d\Omega_p)$ $1p_{1/2}$-state (%)	$1p_{3/2}$-state (%)	$\delta(d^6\sigma/d\omega dE_p d\Omega_e d\Omega_p)$ continuum (%)
0.843	0	2.5	2.6	3.4
	8	0.5	0.4	0.2
	16	0.2	0.9	0.2†
	-8	0.5	0.4	0.3
1.642	0	2.6	2.6	0.8
	8	0.3	0.2	0.2
	-20	0.4	0.1	0.2†
	-16	0.8	1.3	0.2†
	-8	0.7	0.7	0.2
2.442	0	2.5	2.4	1.2
	2.5	1.9	1.9	1.0
	8	0.2	0.2	0.3
	16	0.4	0.5	0.3†
	20	0.2	0.2	0.4†

Table D.8

Uncertainties in the ^{16}O$(e,e'p)$ cross sections due to an uncertainty in the absolute proton momentum of 1.5×10^{-3}. The constraints provided by ^{1}H(e,ep) have not been considered in the above. The $P_{\rm miss}$ bins for which cross sections are reported are presented in Appendix B. Values labelled with a '†' should not be taken too seriously due to the lack of knowledge of the $1s_{1/2}$-state spectral function for $|\theta_{pq}| > 8°$.

$E_{\rm beam}$ (GeV)	θ_{pq} (°)	$\delta(d^5\sigma/d\omega d\Omega_e d\Omega_p)$ $1p_{1/2}$-state (%)	$1p_{3/2}$-state (%)	$\delta(d^6\sigma/d\omega dE_p d\Omega_e d\Omega_p)$ continuum (%)
0.843	0	5.2	3.5	4.6
	8	1.5	1.2	2.4
	16	3.0	5.5	1.3†
	-8	6.1	5.1	6.9
1.642	0	3.9	4.1	1.9
	8	4.3	3.4	6.6
	-20	6.9	0.7	6.0†
	-16	14.3	24.6	6.1†
	-8	10.2	8.3	11.1
2.442	0	4.4	5.6	3.7
	2.5	7.0	8.6	1.3
	8	6.4	5.1	10.1
	16	14.3	26.0	5.1†
	20	5.9	3.1	5.4†

Table D.9

Quadratic sum of the kinematic-dependent systematic uncertainties (see Tables D.4 - D.8) for σ_O which contribute to σ. The constraints provided by ^{1}H(e,ep) have not been considered in the above. The $P_{\rm miss}$ bins for which cross sections are reported are presented in Appendix B. Values labelled with a '†' should not be taken too seriously due to the lack of knowledge of the $1s_{1/2}$-state spectral function for $|\theta_{pq}| > 8°$.

D.2 ^{1}H(e,e)

$E_{\rm beam}$ (GeV)	θ_e (°)	$\delta(d\sigma/d\Omega_e)$ (%)
0.843	100.76	<0.1
1.642	37.17	<0.1
2.442	23.36	<0.1

Table D.10
Uncertainties in the ^{1}H(e,e) cross sections due to an uncertainty in the absolute in-plane electron angle of 0.3 mr. The constraints provided by ^{1}H(e,ep) have been considered in the above. The average uncertainty from this source was <0.1%.